COBEM 2021 26th International Congress of Mechanical Engineering
ABCM Associação Brasileira de Engenharia e Ciências Mecânicas
November 22-26, 2021, Virtual Congress, Brazil

COB-2021-0495
MODELING, IMPLEMENTATION AND APPLICATION OF A TOOL FOR PRELIMINARY HYPERSONIC AIRBREATHING VEHICLE DESIGN

Luiz Henrique Silva Marques Soares
Instituto Tecnológico de Aeronáutica/ITA, Praça Marechal Eduardo Gomes, 50 - Vila das Acacias, CEP 12228-900, São José dos Campos/SP, Brazil
luizlhsms@ita.br

Pedro Paulo Batista de Araújo
Paulo Gilberto de Paula Toro
Universidade Federal do Rio Grande do Norte/UFRN - Centro de Tecnologia. Av. Senador Salgado Filho, 3000 - Campus Universitário, Lagoa Nova, CEP 59.078-970 – Natal/RN - Brazil
araujo.projects@gmail.com, toro11pt@gmail.com

João Felipe de Araújo Martos
Universidade Federal de Santa Maria/UFSM - Centro de Tecnologia. Av. Roraima, 1000 - Cidade Universitária, Camobi, CEP 97105-900 – Santa Maria/RS - Brazil
joao.martos@ufsm.br

Abstract. *In this work, a tool for preliminary hypersonic airbreathing vehicle design, using scramjet technology, was modeled, implemented, and applied. In the initial stages of the design of aerospace systems, it is common to survey the requirements and needs of the design and, subsequently, to define preliminary configurations that can solve doubts, show the existence of problems and be the basis for future details of the systems. Thus, the evaluation of scramjet vehicle planar geometry was determined, and, to evaluate the aerodynamics of the vehicle, considering the hypothesis of perfect gas and inviscid flow, the model was sectioned into the inlet, combustion, and expansion sections applying the respective theoretical-analytical analyzes for each section. For the inlet, the application of the theory of oblique shock wave was considered, and to optimize the geometry, the maximum pressure recovery method was applied to minimize the loss of performance during compression. The combustion section was considered only as a union between the intake and the expansion sections, therefore, the flow with heat addition was disregarded. For the expansion section, the Prandtl-Meyer expansion wave theory was implemented to the point where it was applicable and, subsequently, the area ratio theory was used to finalize the expansion section. Subsequently, in order to verify the effectiveness of the tool, two scramjet vehicle geometries GEO1 and GEO2 were developed, both for flight at 30 km of geometric altitude at the Mach numbers 7 and 10, respectively. Then, in order to compare results, both geometries were evaluated in computational fluid dynamics (CFD) simulations using the ANSYS-Fluent 19.2 code. In the end, with the convergence between analytical and numerical results, the applicability of the tool for preliminary hypersonic airbreathing vehicle design, using scramjet technology was demonstrated. In addition, the resulting differences in geometries were presented when the vehicles are developed for application at different speeds.*

Keywords: *Hypersonic, Airbreathing Propulsion, Scramjet, Oblique Shock Wave, Prandtl-Meyer.*

1. INTRODUCTION

According to Heiser and Pratt (1994), ramjets are engines without moving parts, they do not have rotating components, so there is no need for them to be revolved around a central axis. Designed to operate in flight range in Mach number 3 to 6, ramjet engines are predominantly used in supersonic flights and operate based on the Brayton cycle (Heiser and Pratt, 1994). In addition, appropriately, the engine surfaces are used to compress the flow using oblique shock waves, Figure 1.

From one or more oblique shock waves with the normal shock waves in the diffuser, the supersonic flow is compressed. In this way, considering energy conservation, part of the kinetic energy of the flow is transformed into internal energy and, it results in increase in temperature, pressure, and density of the air, as well as a decrease in the flow velocity for the subsonic regime, to provide propitious characteristics for fuel ignition after its injection. Subsequently, the high-pressure flow is accelerated using a convergent-divergent nozzle to achieve supersonic velocities again.

However, when the flight Mach number exceeds 6, decelerating the flow to the subsonic regime generates very high pressures and temperatures in the combustion chamber, in some cases, above that supported by the structure. To avoid

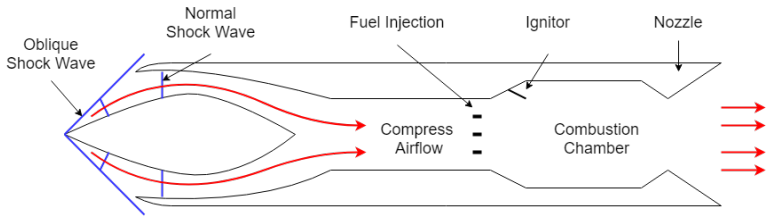

Figure 1: Schematic of ramjet engine (adapted from Corda (2017)).

these problems, a partial compression of the flow is performed using oblique shock waves, preventing the flow in the combustion chamber from becoming subsonic or entering the transonic regime. Thus, there is a ramjet engine with supersonic combustion, that is, a scramjet system, which has better performance for the flight Mach number greater than 6 (Curran (2001)).

Basically, scramjet is a hypersonic integrated airbreathing system, where engine and vehicle are indistinguishable and also has no moving parts and uses oblique/conical shock waves formation to perform the compression and deceleration of the flow, Figure 2.

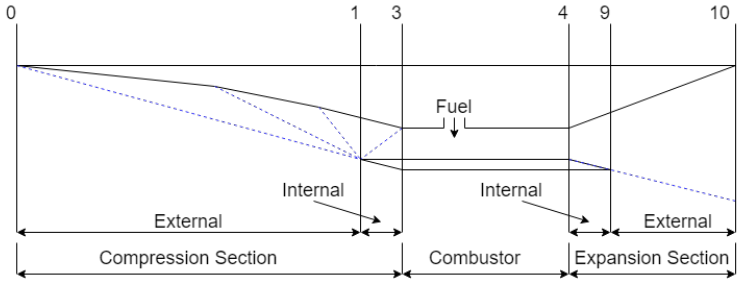

Figure 2: Schematic of scramjet system (adapted from Heiser and Pratt (1994)).

Sectioned according to Figure 2, the compression section (0-3) is responsible for performing the flow compression for a flow with the desired temperature, pressure, and density at the entrance of the combustion chamber, maintaining the supersonic velocity conditions. The combustor section (3-4) is responsible for adding the fuel in the dense flow, with high temperature, pressure, and density and, thus, causing its combustion, without the speed going into a subsonic regime. Finally, the expansion section (9-10) is responsible for expanding the combustor output flow, with a reduction in temperature, pressure, and density and, consequently, an increase in velocity for the supersonic/hypersonic regime (Heiser and Pratt, 1994).

In the initial stages of the design of aerospace systems, it is common to survey the design requirements and needs and, subsequently, the definition of preliminary configurations that can solve doubts, show the existence of problems and be the basis for future details of the systems.

Bonelli *et al.* (2011) described the modeling of a tool, named SPREAD 2.0, used for the preliminary design of a hypersonic airbreathing vehicle. The modeling comprises a plane inlet section, with the presence of oblique shock waves, fuel mixture, combustion process, and plane expansion section. As a differential point, the tool has options such as the variation in the amount of fuel added and shows the influence caused by this variation, for example, how the fuel ratio changes thermodynamic variables and the emission of pollutants.

In this context, this work presents the modeling, implementation, and application of an analytical tool for the optimized preliminary design of hypersonic airbreathing systems, using scramjet technology and its comparison with numerical results.

2. METHODOLOGY

2.1 Design characteristics

First, it is necessary to establish the design characteristics and nomenclature to be used in the development of the scramjet vehicle, Figure 2. When starting the preliminary system design, the application of the system and its main constraints must be known. Thus, in the context of scramjet vehicles, parameters such as flight altitude, flight speed, and possible dimensional restrictions must be known before starting the design.

Regarding the nomenclature used, Heiser and Pratt (1994) present, according to Figure 2, three main components: The compression section (inlet), which has the external and internal regions that are governed by the theory of oblique shock waves and by reflected shock wave, respectively. The combustor, which, in the case of analysis without combustion,

comprises the constant section region that makes the connection between the inlet and the expansion section. Finally, there is the expansion section, divided into internal and external, which are governed by the Prandtl-Meyer expansion theory and ratio area theory.

Therefore, some analyzes are considered to obtain optimized configurations, such as the inlet design by total pressure recovery and a perfectly expanded flow at the nozzle outlet.

2.2 Oblique shock wave theory

According to Anderson (2003), oblique shocks normally occur when a supersonic/hypersonic flow presents a positive direction variation concerning the plane resulting from the surface deflection at a θ angle, Figure 3a. After the deflection, there is a need for flow if adjust as boundary conditions. This adjustment is only possible with the presence of a discontinuity, that is, the shock wave, so that the flow direction adjusts to the surface deflection direction. As the flow experiences the same deflection, equal to the surface deflection, the flow after the shock is uniform and parallel. Across the shock wave, the Mach number reduce, maintaining the supersonic regime, and pressure, temperature, and density increase.

Modeling the flow through the shock wave and considering the simplifications of one-dimensional flow, stationary flow, adiabatic flow, inviscid flow, disregarding body forces, and considering a calorically perfect gas, the equations of Continuity, Momentum, and Energy are obtained. From them and Figure 3b it is possible to obtain the following relationships (Anderson, 2003):

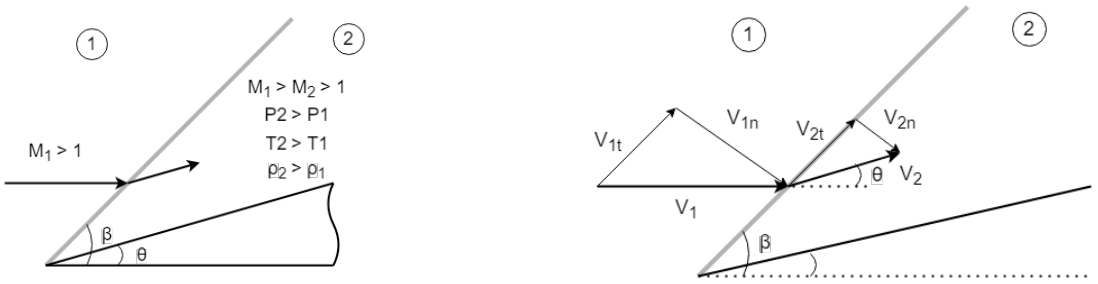

(a) Oblique shock wave.

(b) Velocity diagram in a oblique shock wave

Figure 3: Oblique Shock Wave analysis.

- Normal Mach number before oblique shock wave:

$$M_{1_n} = M_1 sen\beta; \tag{1}$$

- Pressure ratio through oblique shock wave:

$$\frac{p_2}{p_1} = 1 + \frac{2\gamma}{\gamma+1}\left(M_{n_1}^2 - 1\right); \tag{2}$$

- Density ratio through oblique shock wave:

$$\frac{\rho_2}{\rho_1} = \frac{(\gamma+1)M_{n_1}^2}{(\gamma-1)M_{n_1}^2 + 2}; \tag{3}$$

- Temperature ratio through oblique shock wave:

$$\frac{T_2}{T_1} = \frac{p_2}{p_1}\frac{\rho_1}{\rho_2}; \tag{4}$$

- Normal Mach number after oblique shock wave:

$$M_{n_2}^2 = \frac{M_{n_1}^2 + [2/(\gamma-1)]}{[2\gamma/(\gamma-1)]M_{n_1}^2 - 1}; \tag{5}$$

- The relationship between the surface angle θ and the angle of the oblique shock wave β given as a function of the specific heat ratio γ (calorically perfect air, γ = 1.4) and the Mach number incident on the shock wave:

$$\tan\theta = 2\cot\beta\left[\frac{M_1^2\sin^2\beta - 1}{M_1^2(\gamma + \cos 2\beta) + 2}\right]; \tag{6}$$

- Mach number after oblique shock:

$$M_2 = \frac{M_{n_2}}{\sin(\beta - \theta)}; \tag{7}$$

2.3 Total pressure recovery theory

The performance and operation of the hypersonic airbreathing vehicles are significantly affected by the flow quality. According to Ran and Mavris (2005), the loss of total pressure directly influences the decrease in thrust and, consequently, the increase in fuel consumption. These suggest a methodology for maximizing the total pressure applied to a supersonic inlet geometry.

In general, the methodology proposed by Oswatitsch (1947) and applied to the hypersonic scramjet inlet by Martos (2017) suggests that in a system with n-1 incident oblique shock waves, Figure 4, the maximum recovery of total pressure is achieved when the shock waves have the same intensity, that is, when the normal component of the velocity in the shock wave is equal in all incident waves.

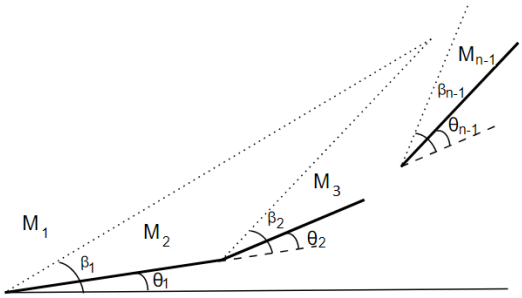

Figure 4: Schematic of supersonic inlet (adapted from Ran and Mavris (2005)).

Thus, considering the normal component in oblique shock waves, the equation is given by

$$M_1 sin\beta_1 = M_2 sin\beta_2 = M_{n-1} sin\beta_{n-1}. \tag{8}$$

Finally, the total pressure ratio across the oblique shock wave, presented by Heiser and Pratt (1994), is defined as

$$\Pi = \frac{p_{out}}{p_{in}} \left\{ \frac{1 + \frac{\gamma-1}{2} M_{out}^2}{1 + \frac{\gamma-1}{2} M_{in}^2} \right\}^{\gamma/(\gamma-1)}. \tag{9}$$

2.4 Reflected oblique shock wave

According to Anderson (2003) and Figure 5, when an oblique shock wave strikes a solid surface, the reflection of the incident wave occurs, normally called a reflected oblique shock wave. Similarly, to the incident oblique wave theory, the flow fits the boundary conditions of the surface, becoming parallel to it.

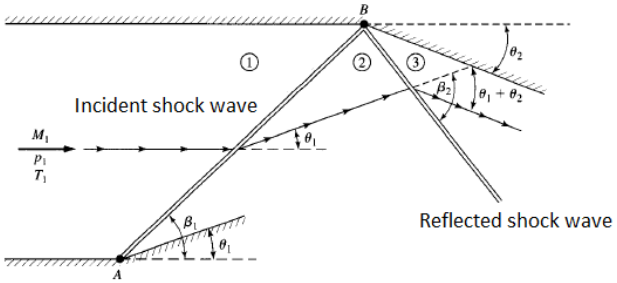

Figure 5: Schematic of reflected shock wave (adapted from Anderson (2003).)

Oblique shock wave theory is used for incident shock waves and also for the reflected shock wave.

2.5 Combustor Considerations

In this article, by disregarding the phenomenon of combustion, the combustor will play the role of connecting the flow of the compression section with an expansion section. If combustion is considered, according to Anderson (2003), the theory of one-dimensional flow with added heat (Rayleigh flow) is normally used.

However, the desired flow properties at the entrance to the combustor are design parameters for a compression section.

2.6 Prandtl-Meyer and area ratio theories

According to Heiser and Pratt (1994), the main function of the expansion system and its components is to provide acceleration to the proven flow from the combustor in a more efficient way, that is, with a minimum increase in entropy.

Considering an inviscid flow and a calorically perfect gas, it is considered that the uniform supersonic flow from the combustion chamber reaches an expansion region formed, initially, by Prandt-Meyer expansion wave that is the result of a divergent variation of the geometry, Figure 6.

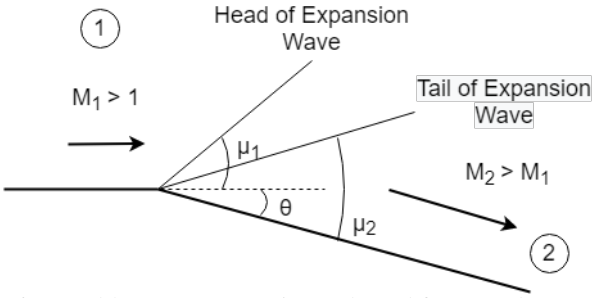

Figure 6: Prandtl-Meyer Expansion (adapted from Anderson (2003)).

θ is the deflection angle of the expansion geometry given by

$$\theta = \nu(M_2) - \nu(M_1), \tag{10}$$

where a Prandtl-Meyer function ν(M) is presented as a function of the Mach number per

$$\nu(M) = \sqrt{\frac{\gamma+1}{\gamma-1}} tg^{-1} \sqrt{\frac{\gamma-1}{\gamma+1}\left[M^2-1\right]} - tg^{-1}\sqrt{M^2-1}. \tag{11}$$

Furthermore, ν_1 and ν_2 are the Mach wave angles calculated by

$$\mu_n = \arcsin\frac{1}{M_n}. \tag{12}$$

Once the Mach number M_2 after the expansion wave is characterized, the ratio between the flow properties are inherited, according to Anderson (2003), by the isentropic relationships

$$\frac{T_2}{T_1} = \left(\frac{1+\frac{\gamma-1}{2}M_1^2}{1+\frac{\gamma-1}{2}M_2^2}\right), \tag{13}$$

$$\frac{p_2}{p_1} = \left(\frac{T_2}{T_1}\right)^{\frac{\gamma}{\gamma-1}}, \tag{14}$$

$$\frac{\rho_2}{\rho_1} = \left(\frac{T_2}{T_1}\right)^{\frac{1}{\gamma-1}}. \tag{15}$$

However, according to Heiser and Pratt (1994), the theory of expansion wave of Prandtl-Meyer is valid only for confined flows, that is, when the existence of reflection of the wavefronts is possible. Thus, for expansions defined as external, it is necessary to use the area ratio theory, presented in Anderson (2003), which has an analytical equation given by

$$\frac{A_2}{A_1} = \frac{M_1}{M_2}\left(\frac{1+\frac{\gamma-1}{2}M_2^2}{1+\frac{\gamma-1}{2}M_1^2}\right)^{\frac{\gamma+1}{2(\gamma-1)}}. \tag{16}$$

Figure 7 presents a schematic of the expansion section containing the Prandtl-Meyer and area ratio theories. The main difficulty of the process is to determine the region where the Prandtl-Meyer theory is valid.

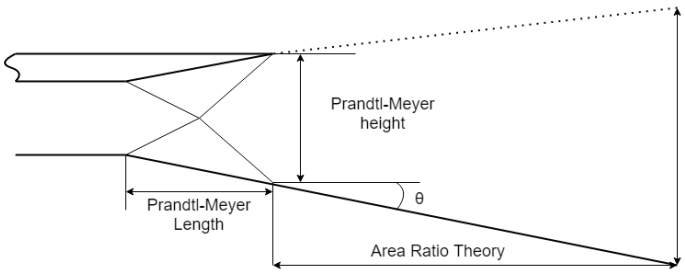

Figure 7: Schematic of expansion section.

3. TOOL MODELING

To provide the modeling of the system with less computational use and more intuitively, it is necessary to break it down into subsystems. Aiming at a study consisting of determining the inputs and outputs of each subsystem, it was decided to section the modeling according to Figure 8, which includes the subsystems considered in the vehicle.

The design parameters comprise the definition of flight speed, flight altitude and thermodynamic properties of free flow determined according to Atmosphere (1976). From the definition of the number of ramps and the estimate for the angle of the first ramp, the first oblique shock wave is defined and the thermodynamic properties of the flow after the first shock wave are calculated. From this, considering the theory of maximum total pressure recovery, the next ramps and the next shock waves are determined. Subsequently, the reflected shock wave is calculated and thus the properties at the input of the combustor are determined. If the properties found are different from those desired, increments are made in the angle of the first ramp until the desired thermodynamic properties at the input of the combustor are found. The length of the ramps is set so that the oblique shock waves strike the leading edge of the cowl (shock on-lip) and the reflected shock wave hits the combustor inlet (shock on-corner). Finally, as there is no combustion, the Prandtl-Meyer theory is used for expansion of the confined flow and the Area Ratio Theory to finish the expansion section considering a perfectly expanded flow at the exit of the nozzle, that is, the outlet pressure equals freestream pressure.

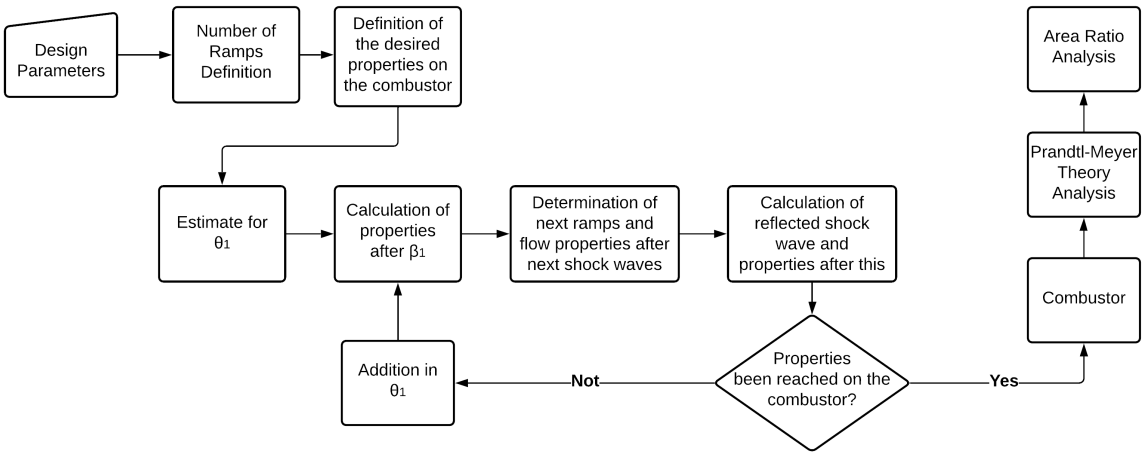

Figure 8: Schematic of scramjet preliminary design tool.

4. RESULTS AND COMMENTARIES

4.1 Analytical Results

To demonstrate the flexibility of the tool, two case studies were developed: A geometry for flight at Mach number 7 (GEO1) and another geometry for flight at Mach number 10 (GEO2), both at 30 km of geometric altitude.

Initially, it is necessary to determine the thermodynamic properties of the air for 30 km of geometric altitude, Table 1.

Table 1: Thermodynamic atmospheric properties at 30 km altitude (Atmosphere, 1976).

Geometric Altitude (Z) [km]	**Temperature (T)** [K]	**Pressure (p) [Pa]**	**Density (ρ) [kg/m^3]**	**Speed of Sound (a) [m/s]**
30	226.5	1197	0.01841	301.7

Later, in defining the number of ramps, Martos (2017) analyzes the relationship between the number of ramps and the efficiency of compression and determination, based on the total pressure recovery methodology and considering the effects of manufacturing complexity, that a system with three ramps is the ideal point between efficiency and complexity. Similarly, considering the data provided by Martos (2017) as a reference, the necessary temperature of 1100 K at the entrance of the combustion chamber and the vehicle height of 0.38 m were estimated. To estimate the length of the combustor, based on the scramjet vehicle detailed in Martos (2017), it was considered that the flow remained inside the combustor for 0.1 ms.

From the modeled computational routine and considering the stipulated design definitions, geometric results were obtained for vehicles GEO1 and GEO2, Tables 2 and 3, respectively.

Table 2: GEO1 vehicle geometric results.

Geometry GEO1						
	Ramp 1	**Ramp 2**	**Ramp 3**	**Reflection (Combustor)**	**Expansion**	**Total**
θ	6.124º	7.238º	8.609º	21.971º	15.674º	-
β	12.777º	15.186º	18.218º	34.399º	-	-
Length	0.486 m	0.216 m	0.206 m	(0.1645 m)	0.639 m	1.6898 m

Table 3: GEO2 vehicle geometric results.

Geometry GEO2						
	Ramp 1	**Ramp 2**	**Ramp 3**	**Reflection (Combustor)**	**Expansion**	**Total**
θ	4.222º	4.936º	5.786º	14.945º	8.917º	-
β	8.842º	10.359º	12.184º	22.390º	-	-
Length	0.687 m	0.308 m	0.313 m	(0.271 m)	1.151 m	2.715 m

The results of the thermodynamic properties of GEO1 and GEO2 vehicles were also collected, Tables 4 and 5, respectively.

Table 4: results of thermodynamic properties along GEO1.

	M [-]	**p [Pa]**	**T [K]**	**ρ[kg/m^3]**	**a [m/s]**
Freestream	7	1197	226.5	0.01841	301.7
Ramp 1	5.909	3147.510	306.358	0.0357	350.848
Ramp 2	4.951	8276.375	414.356	0.0695	408.030
Ramp 3	4.101	21762.723	560.426	0.1352	474.530
Combustor In/Out	2.473	132722.114	1100.001	0.4203	664.816
Expansion Section (Prantdl-Meyer)	3.240	41513.913	789.185	0.1832	563.111
Expansion Section (Area Ratio)	6.139	1197.0	286.517	0.01455	339.297

First, it should be noted that the design criterion that determined the minimum required temperature of 1100 K at the entrance of the combustor was reached in both geometries. It is observed that the scramjet concept was maintained by presenting a Mach number at the combustor entrance of 2.473 for the GEO1 geometry and 4.076 for the GEO2 geometry. In both cases, the optimization criterion for total pressure recovery was correctly applied. Furthermore, about the expansion of the gases, a perfectly expanded regime was obtained, since the outlet pressure is equal to the freestream pressure of 1197.0 Pa.

Regarding the differences between the geometries, it appears that for the same design criterion, when increasing the Mach number, ramps with smaller angles are needed to compress the flow, but it results in a longer vehicle. This fact can lead to problems when considering the effects of viscosity (presence of the boundary layer).

Table 5: results of thermodynamic properties along GEO2.

	M [-]	p [Pa]	T [K]	ρ[kg/m^3]	a [m/s]
Freestream	10	1197	226.5	0.01841	301.7
Ramp 1	8.547	3100.030	304.672	0.0354	349.881
Ramp 2	7.282	8028.563	409.807	0.0682	405.784
Ramp 3	6.176	20792.641	551.223	0.1314	470.618
Combustor In/Out	4.076	130807.020	1100.040	0.4142	664.827
Expansion Section (Prantdl-Meyer)	4.872	48286.466	827.465	0.2033	576.606
Expansion Section (Area Ratio)	8.812	1197.0	287.719	0.0144	340.008

4.2 Numerical Results

To compare the analytical results obtained with the numerical solutions of the Navier-Stokes equations, the vehicles were modeled and analyzed in the ANSYS - Fluent 19.2 CFD code. Figure 9 presents the defined 2D domain and the main features used for the analysis of the GEO1 geometry.

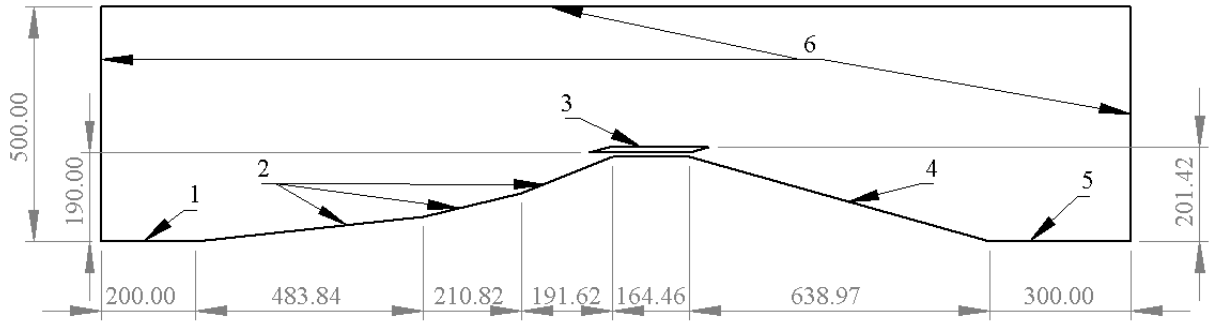

Figure 9: GEO1 geometry dominion.

To nullify the boundary effects in the simulation, a domain larger than the vehicle dimensions was considered. For this, they were modeled, horizontally, the surfaces 1 and 5 and, vertically, the region 6 to compose the appropriate domain for the simulation.

For the analysis of the GEO2 geometry, the domain, Figure 10, was defined in a similar way.

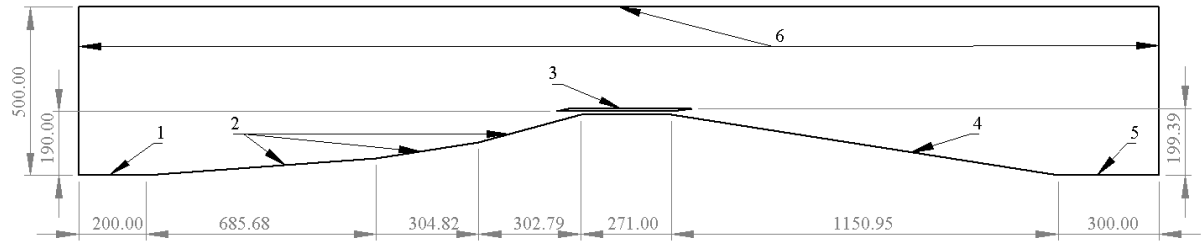

Figure 10: GEO2 geometry dominion.

In the definition of the mesh, since it is an inviscid analysis, a triangular mesh with a maximum element size of 10 mm was considered. To generate an adequate mesh, we used the definition of the size of the elements on the surfaces of interest of the vehicle.

For the GEO1 geometry, according to Figure 9, on the surfaces that make up regions 2 and 4, an element size wall as defined with 0.75 mm, on the horizontal surfaces of region 3, an element size wall as defined with 0.3 mm elements and on slanted surfaces, 0.2 mm elements. From the defined surfaces, the size of the elements grows from a rate of 1.0125 until contemplating the entire defined domain, Figure 11.

Due to the geometries have similar dimensions, in the GEO2 geometry, the same mesh design conditions were considered, Figure 12.

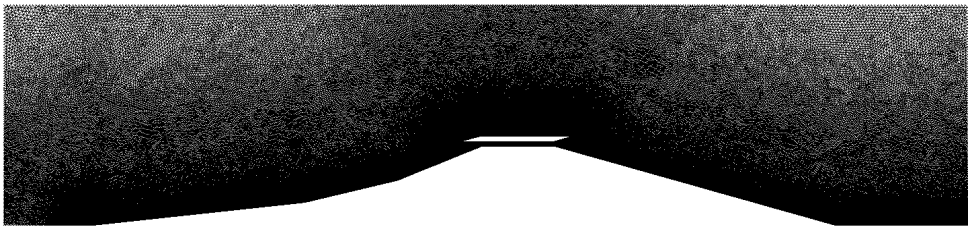

Figure 11: GEO1 geometry dominion initial mesh.

Figure 12: GEO2 geometry dominion initial mesh.

In both configurations of the numerical analysis, planar 2D space and ideal gas were considered. For the definition of the boundary conditions, according to Figures 9 and 10, surfaces 1 and 5 were considered as symmetry, the surfaces that make up regions 2, 3, and 4, as the wall and the surfaces of region 6 as the pressure far field where the ambient and operating conditions of the vehicle was defined.

For the mesh refinement, in both geometries, the adaptation of the elements from the pressure gradient criterion was used, that is, the mesh was refined where the presence of pressure variation was verified. As, in this case, the pressure variation occurs mostly in the regions of shock waves and expansion waves, the criterion used was considered adequate to define the position of the shock waves more precisely, Figure 13.

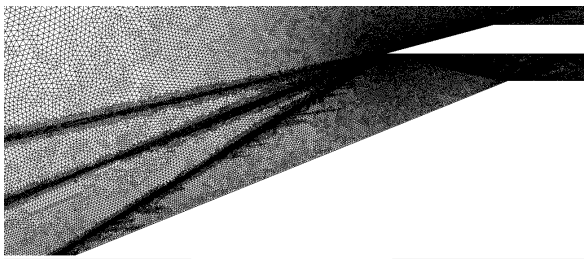

Figure 13: GEO1 geometry dominion mesh refinement example.

The results for the GEO1 geometry can be seen in Figures 14a and 14b and in Figure 15a and 15b for the GEO2 geometry where the color spectrum is presented as a function of the Mach number.

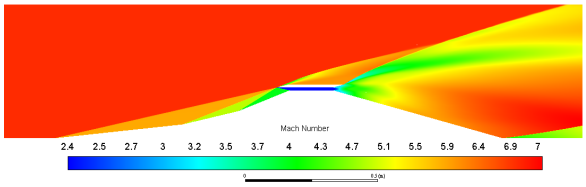

(a) Global view in function of Mach number.

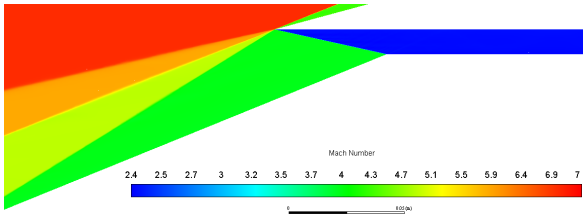

(b) Shock on-lip and on-corner in function of Mach number.

Figure 14: GEO1 results of numerical analysis.

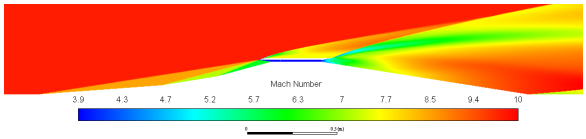

(a) Global view in function of Mach number.

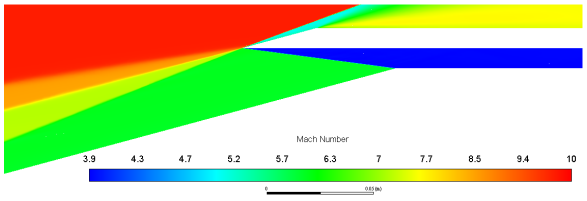

(b) Shock on-lip and on-corner in function of Mach number.

Figure 15: GEO2 results of numerical analysis.

In both geometries, in the visual results of the numerical analysis, it is possible to visualize the gradual decrease of the Mach number as expected by the total pressure recovery optimization criterion. It is verified that the length of the ramps was properly defined according to the presence of shock on-lip and shock on-corner.

Furthermore, as there is no combustion, the flow with a constant Mach number inside the combustor is verified. In the end, the expansion process of the gases presented by the gradual increase in the Mach number is observed.

Analyzing the numerical results graphically and comparing them with the analytical results Figures 16 and 17, in both cases there is a convergence between the methods for the highlighted thermodynamic variables, demonstrating the flexibility of the analytical tool when developing different geometries.

However, there is a small divergence between the analyzes in the expansion section, they are explained by analytical approaches that are made when considering the area ratio theory. To analyze with more detail, the Method of Characteristics, for example, can be used. In addition, the flow outside the vehicle influences in the flow of the expansion region, and is difficult to predict this phenomenon in analytical analysis.

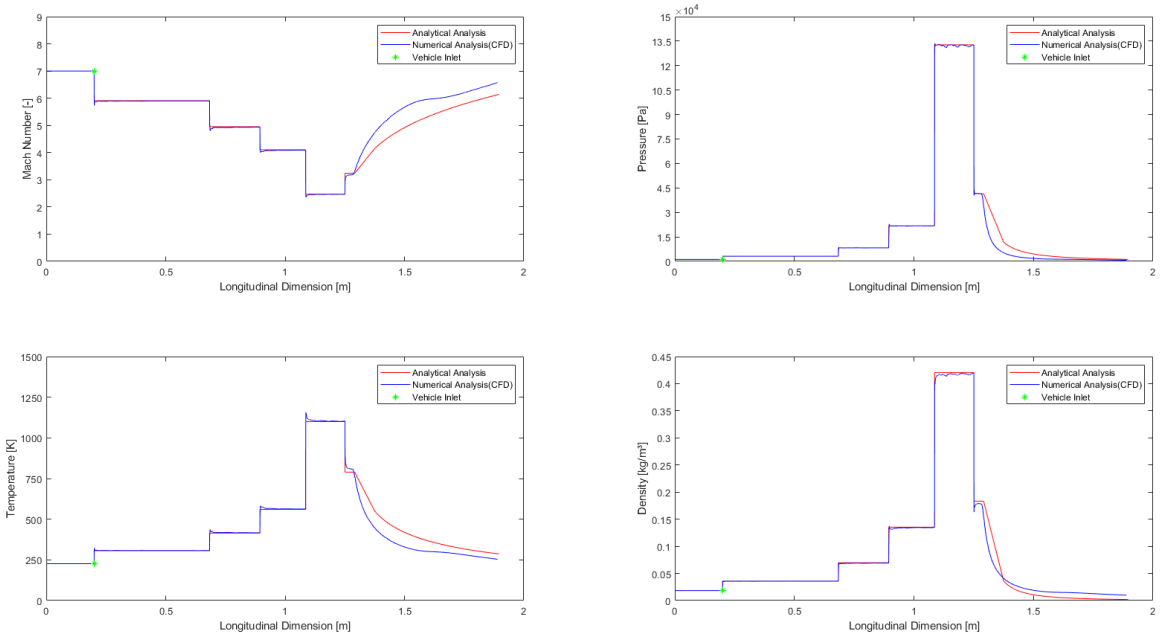

Figure 16: Comparison between analytical and numerical thermodynamic properties for GEO1.

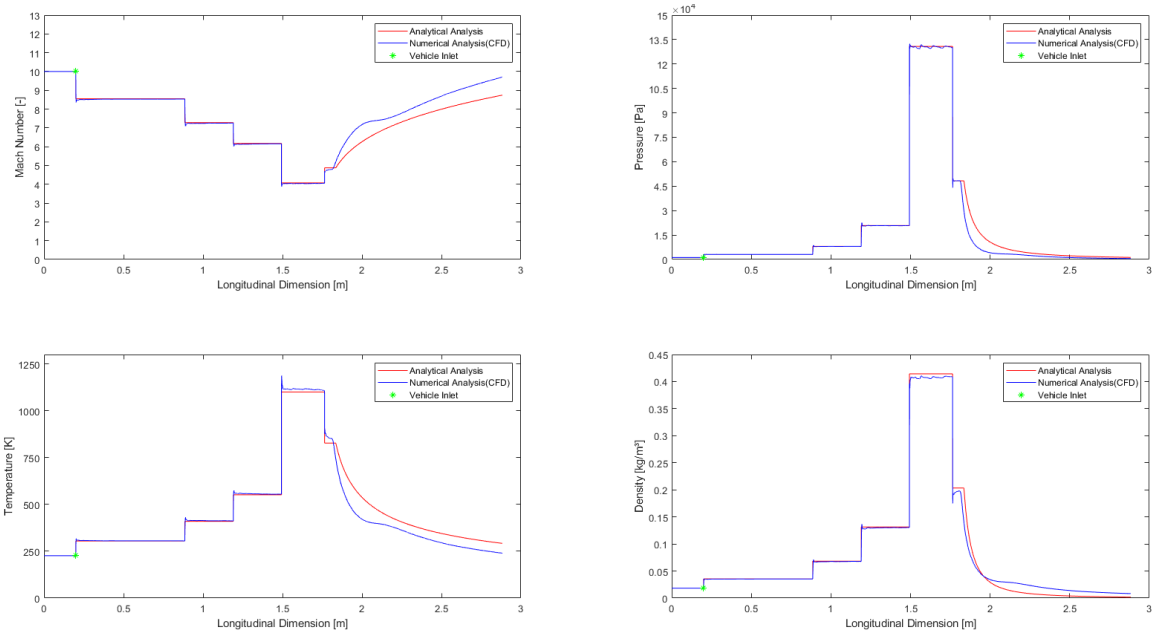

Figure 17: Comparison between analytical and numerical thermodynamic properties for GEO2.

5. CONCLUSION AND OUTLOOK FOR FUTURE DESIGNS

A preliminary design tool for hypersonic airbreathing vehicles using scramjet technology was developed. Criteria for optimizing the recovery of the total pressure in the compression section and the perfectly expanded flow at the nozzle outlet were used as a basis.

The formulation based on the definition of initial requirements for design such as altitude and flight speed, desired characteristics at the entrance of the combustor, as well as the definition of dimensional criteria, such as vehicle height.

Two geometries were generated, GEO1 and GEO2, for flight Mach numbers 7 and 10, respectively, to evaluate the results obtained by the tool and compare them with numerical results. It was observed that both geometries met the design requirement that the supersonic flow should reach a minimum temperature of 1100 K at the combustor entrance. It was also verified that in both cases the definition of the length of the ramps was adequate to result in shock on-lip and shock on-corner. By optimizing the angle of the expansion ramps, it was possible to obtain a perfectly expanded flow at the nozzle outlet, since the gas outlet pressure was equal to the freestream pressure, 1197.0 Pa.

When comparing the analytical results with the numerical results obtained from the ANSYS-Fluent 19.2 Code it was verified convergence in the compression section and the combustor. However, there was a small divergence in the expansion region are explained by approximations made when considering the area ratio theory and by the influence of external flow on the expansion flow.

In the end, the flexibility of the tool in generating optimized geometries for certain design criteria is verified. However, for a more assertive preliminary analysis, it is necessary to realize numerical analysis and consider the effects of viscosity (presence of the boundary layer), the influence of combustion in changing the thermodynamic properties of the flow, and the effects of real gas. Thus, it will be possible to evaluate aspects such as thrust generation.

6. ACKNOWLEDGEMENTS

This study was financed in part by the Coordenação de Aperfeiçoamento de Pessoal de Nível Superior - Brasil (CAPES) - Finance Code 001. Also, the authors would like to thank CAPES the support given by the Project PROCAD-DEFESA 88887.626266/2021-00. The authors would like to thank the Instituto Tecnológico de Aeronáutica (ITA), Universidade Federal do Rio Grande do Norte (UFRN) and a Universidade Federal de Santa Maria (UFSM) to support granted to carry out research on hypersonic airbreathing propulsion.

7. REFERENCES

Anderson, J.D., 2003. *Modern compressible flow: with historical perspective*. McGraw-Hill Education.

Atmosphere, U.S., 1976. *NASA TM-X 74335*.

Bonelli, F., Cutrone, L., Votta, R., Viggiano, A. and Magi, V., 2011. "Preliminary design of a hypersonic air-breathing vehicle, 2011". *17th AIAA International Space Planes and Hypersonic Systems and Technologies Conference*.

Corda, S., 2017. *Introduction to aerospace engineering with a flight test perspective*. John Wiley & Sons.

Curran, E.T., 2001. "Scramjet engines: the first forty years". *Journal of Propulsion and Power*, Vol. 17, No. 6, pp. 1138–1148.

Heiser, W.H. and Pratt, D.T., 1994. *Hypersonic airbreathing propulsion*. AIAA.

Martos, J., 2017. *Aerothermodynamic Design, Manufacture And Testing Of a 3-D Prototyped Scramjet*. Doctor in science in the program of space science and technology, area of space propulsion and hypersonics, Instituto Tecnológico de Aeronáutica, São José dos Campos.

Oswatitsch, K., 1947. "Pressure recovery for missiles with reaction propulsion at high supersonic speeds (the efficiency of shock diffusers)". *NACA Technical Memorandum*, Vol. 1140.

Ran, H. and Mavris, D., 2005. "Preliminary design of a 2d supersonic inlet to maximize total pressure recovery". *AIAA 5th Aviation, Technology, Integration, and Operations Conference (ATIO)*, p. 11.

8. RESPONSIBILITY NOTICE

The authors are the only responsible for the printed material included in this scientific article.

The authors declare that there is no conflict of interest regarding the publication of this scientific article.